



Empirical Site Amplification Modeling for Taiwan

Chun-Hsiang Kuo⁽¹⁾, Shu-Hsien Chao⁽²⁾, Che-Min Lin⁽³⁾, Jyun-Yan Huang⁽⁴⁾, Kuo-Liang Wen⁽⁵⁾

⁽¹⁾ *Researcher, National Center for Research on Earthquake Engineering, Taiwan, chkuo@ncree.narl.org.tw*

⁽²⁾ *Assistant Researcher, National Center for Research on Earthquake Engineering, Taiwan, shchao@ncree.narl.org.tw*

⁽³⁾ *Researcher, National Center for Research on Earthquake Engineering, Taiwan, cmlin@narlabs.org.tw*

⁽⁴⁾ *Assistant Researcher, National Center for Research on Earthquake Engineering, Taiwan, jyhuang@narlabs.org.tw*

⁽⁵⁾ *Professor, National Central University, Taiwan, wenkl@cc.ncu.edu.tw*

Abstract

Characteristics of site amplifications caused by moderate to large earthquakes are important in ground motion prediction. Seismic waves were usually amplified and caused significant building damages especially in the Taipei Basin during the 1986 Hualien offshore (subduction interface) and the 1999 Chi-Chi earthquakes (crustal), for which both of the epicentral distances were nearly 100 km. To understand site amplification behaviors in Taiwan, empirical site amplification factors for both horizontal and vertical ground motions are studied using recently constructed strong motion and site databases for the free-field TSMIP stations. Records of large magnitude earthquakes of M_w larger than 5.5 from 1991 to 2014 were selected for this study. Site amplification factors at site conditions with V_{s30} between 150 m/s to 1500 m/s and bedrock accelerations up to 0.8 g were evaluated using ratios of PGA, PGV, and spectral accelerations at different periods. The reference site condition, i.e. the engineering bedrock, is assumed as V_{s30} of 760 m/s (B/C boundary) in this study. Our empirical site amplification model borrowed the site response function from ASK14 and CY14 ground motion models in NGA-West2 project with slight modification. Therefore our site amplification model includes a linear amplification term and a nonlinear deamplification term. The coefficients of the empirical models were obtained by a nonlinear regression analysis using selected Taiwan data. Site amplification factor is a function of V_{s30} and spectral intensity in the model. Similar linear site amplification factor to the NGA models is evaluated; however, more significant soil nonlinearity behavior than the NGA models is likely found from the empirical data.

Keywords: empirical site amplification model, soil nonlinearity, ground motion



1. Introduction

Characteristics of ground motions are the summary of seismic source, path, and site effect. After the destructive large earthquakes occurred in the past decades, such as the 1985 Mexico [1], 1986 Hualien Offshore, 1989 Loma Prieta, and 1999 ChiChi, seismologists have focus on the site amplification behavior of ground motions. Experimental and analytical methods of using both seismic and microtremor records have been conducted to discuss site effect [2, 3, 4].

Engineer Seismologists have improved site classifications by V_s30 (average shear-wave velocity of the top 30 meters) instead of surficial geology. V_s30 is a continuous number and suitable for quantitative analysis of site amplifications.

Borcherdt [5] studied site amplifications of ground motions during the 1989 Loma Prieta earthquake using borehole-geotechnical data and ground motion measurements to account for local geological conditions in seismic design code. This study analyzed relationships between site amplifications and V_s30 in different intensity levels. The result had been adopted by National Earthquake Hazards Reduction Program (NEHRP) in the seismic design code of Building Seismic Safety Council (BSSC) [6]. Borcherdt [7] used more seismic data from the 1994 Northridge earthquake to further clarify decrease of site amplification factors with increasing base accelerations.

2. Data Acquisition

A reevaluation of probabilistic seismic hazard of nuclear facilities in Taiwan using SSHAC Level 3 methodology project [8] was conducted by National Center for Research on Earthquake Engineering (NCREE) since 2015. A strong motion database was therefore constructed to meet requirement of the project. Brief introduction of the datasets collected in the strong motion database was described as in the following section.

The Central Weather Bureau (CWB) embarked on the seismic strong motion instrumentation program, known as the Taiwan Strong Motion Instrumentation Program (TSMIP) since 1991 [9]. More than 800 free-field strong motion stations have been installed, which give high-quality instrumental recordings of strong motions. The strong motion database is constructed for evaluating existing ground motion prediction equation (GMPE) and developing new GMPE. The selected earthquakes are therefore classified as crustal, subduction interface, and subduction intraslab according to the locations. Focal mechanism of each event is also provided. The intensity measures include PGA, PGV, PGD, and pseudo-spectral acceleration (PSA) at periods from 0.01 sec to 20 sec for both horizontal and vertical components. The processing method of the strong ground motion data of this strong motion database basically follows the processing method and flow of the NGA project. The horizontal intensity measures are rotated to RotD50 (50 percentile values of response spectra of the two horizontal components projected onto all nonredundant azimuths) [10]. Fig. 1 shows the locations of crustal (left) and subduction (right) earthquakes included in the strong motion database of NCREE. The panels in the right and below show the focal depth with latitude and longitude. Moment magnitude of events are noted by different colors. Different symbols indicate focal mechanisms for crustal events and types for subduction events.

At present, 463 of 816 TSMIP free-field strong motion stations have completed drilling geological survey and shear wave velocity measurements [11]. Kuo et al. [12] compiled measured [11, 13] and estimated [14, 15] V_s30 for all TSMIP free-field strong motion stations. Strong motion recordings observed by other networks such like Strong Motion Array in Taiwan, phase I (SMART1), phase II (SMART2), and Broadband Array in Taiwan for Seismology (BATS) were also selected into the strong motion database; however, those seismic stations are lack of reliable site conditions and was not used in the present study. The V_s30 map (left) and the station distribution (right) are plotted in Fig. 2. Kuo12 [11] and Kuo16 [13] are measured V_s30 denoted as blue dots whereas Kwok18 [14] and Lin18 [15] are estimated V_s30 denoted as green and red dots.

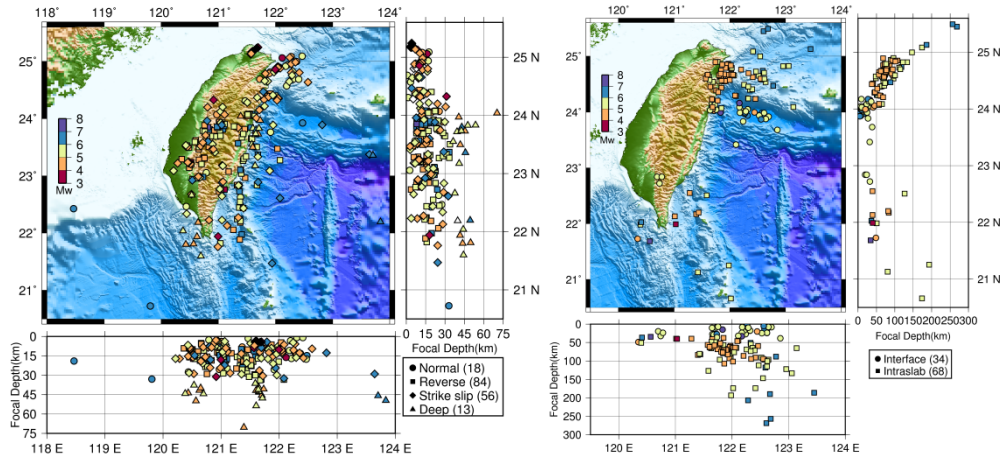


Fig. 1 – Earthquakes collected in the strong motion database of NCREE.

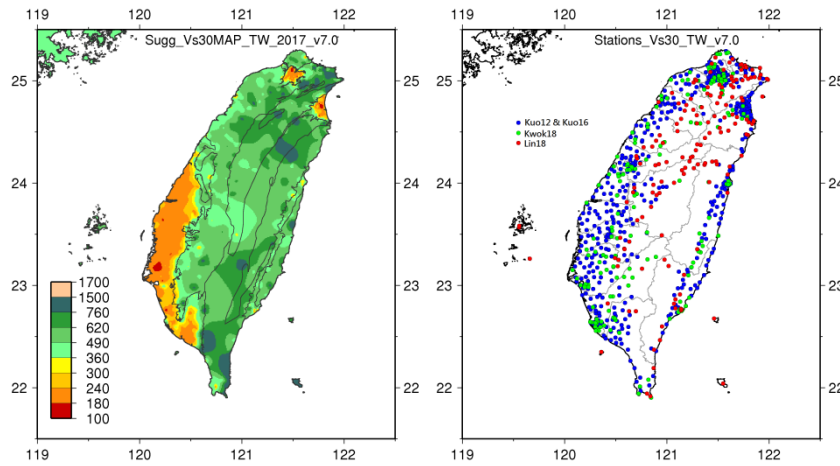


Fig. 2 – Vs30 map and the station locations.

3. Methodology and Empirical Model

Standard Spectral Ratio (SSR) is a widely used method to analyze seismic site amplifications [2, 5, 7], which we also adopted in this study.

$$A(f) = S_0(f) \times P(f) \times S_1(f) \quad (1)$$

where the $A(f)$ is a intensity measure of ground motions, $S_0(f)$, $P(f)$, and $S_1(f)$ are source, path and site effects, respectively. The amplification factors can be derived via the SSR,

$$AF = \frac{A(f)_{targ.}}{A(f)_{ref.}} = \frac{S_1(f)_{targ.}}{S_1(f)_{ref.}} \quad (2)$$

where the $A(f)_{targ.}$ is the ground motion at target site, the $A(f)_{ref.}$ is the ground motion at a nearby reference rock site during same earthquake, and AF is the derived amplification factor.

The site condition of reference rock is assumed as Vs30 of 760 m/s (B/C boundary) in this study. We selected the stations with measured Vs30 from 600 m/s to 900 m/s as the reference rock sites in practical. The distance between station pairs which used to calculate amplification factors has to be less than 10 km. Amplification factors were therefore derived according to the criteria described above.



We selected events of M_w larger than 5.5 and only those were observed by reference rock sites and nearby stations (distance less than 10 km) simultaneously can be used in this study. Fig. 3 shows the epicenters of the crustal and subduction earthquakes used in this study. About half of the crustal earthquakes were occurred inland and the others occurred offshore. Most subduction earthquakes occurred offshore and only few occurred inland due to the subduction zones extend to depth under the Taiwan island. The selected horizontal strong motion datasets were displayed in Fig. 4. Left shows event magnitude with base PGA at rock sites. Right shows V_{s30} with observed PGA. Therefore site amplification factors at site conditions with V_{s30} between 150 m/s to 1500 m/s and bedrock accelerations up to 0.8 g were evaluated using SSR of PGA, PGV, and spectral accelerations at different periods. Same procedure was also applied to vertical component for evaluation of vertical site response model. Fig. 5 shows the same selected strong motion datasets as Fig. 4 but for vertical component.

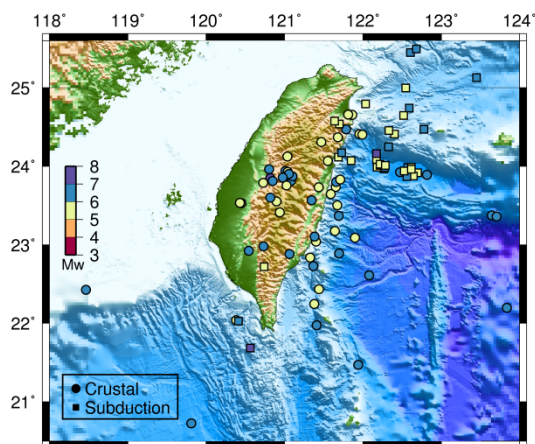


Fig. 3 – Epicenters of events used in this study.

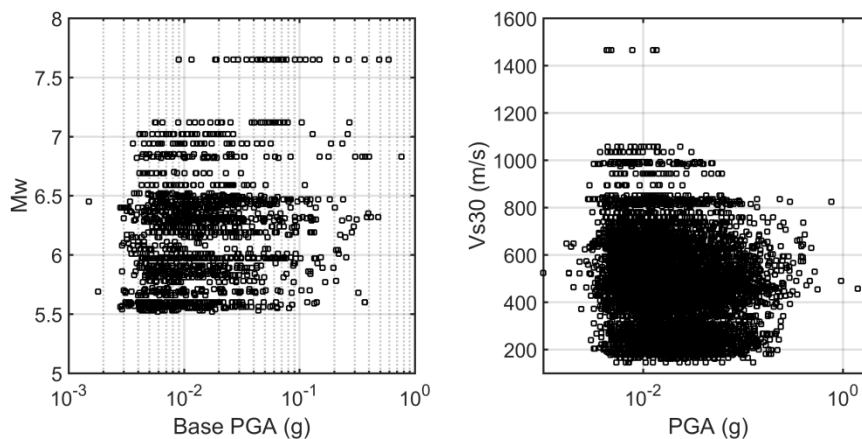


Fig. 4 – Selected horizontal ground motion datasets used in this study.

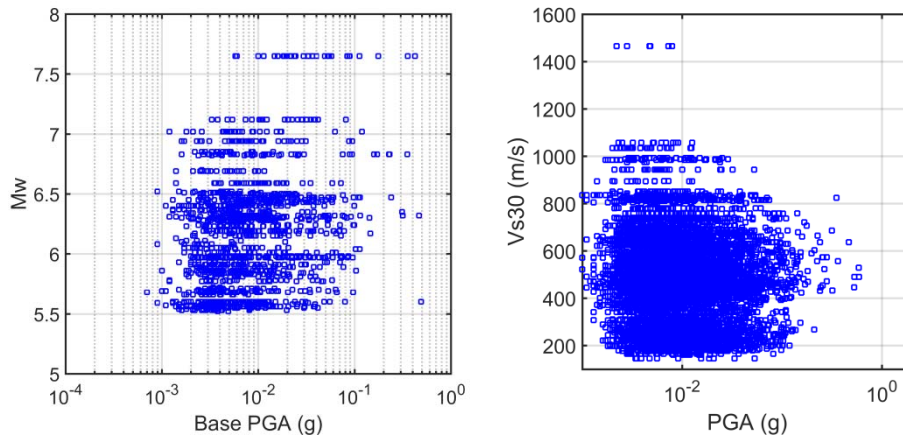


Fig. 5 – Selected vertical ground motion datasets used in this study.

A traditional amplification model used by Borchardt [5, 7] and adopted by building code [6] was like Eq. (3).

$$AF = (a/Vs30)^b \quad (3)$$

where a and b are coefficients, and $Vs30$ denotes the reference site condition. However, the model can only express relationship between amplification factor and $Vs30$. Several models are needed to explain different amplification behaviors with increasing intensities.

Several site response models [16, 17, 18] were introduced in NGA-West2 project. Our empirical site amplification model borrowed the site response function form from ASK14 [16] and CY14 [17] ground motion models with slight modification. Consequently our site amplification model includes a linear amplification term and a nonlinear deamplification term. The coefficients of the empirical models were obtained by a nonlinear regression analysis using selected Taiwan data from the strong motion database of NCREC. Eq. (4) to Eq. (6) demonstrate the site response model used in this study.

$$\ln(AF) = \ln(F_{lin}) + \ln(F_{nl}) \quad (4)$$

$$\ln(F_{lin}) = \begin{cases} \phi_1 \ln\left(\frac{Vs30}{760}\right) & Vs30 \leq Vc \\ \phi_1 \ln\left(\frac{Vc}{760}\right) & Vs30 > Vc \end{cases} \quad (5)$$

$$\ln(F_{nl}) = \phi_2 \left[e^{\phi_3(\min(Vs30, 760) - 360)} - e^{\phi_3(760 - 360)} \right] \cdot \ln\left(\frac{y_{ref_ij} + \phi_4}{\phi_4}\right) \quad (6)$$

The model consist of a linear term ($\ln(F_{lin})$) and a nonlinear term ($\ln(F_{nl})$), which account for linear amplification and nonlinear deamplification in different intensities. Vc in Eq. (5) changes with periods indicating a upper bound of shear wave for nonlinear site effect. The y_{ref_ij} is intensity of reference rock sites. $\phi_1 \sim \phi_4$ are four coefficients derived from the regression analysis. Compared with traditional model as described in Eq. (3), the new model incorporates nonlinear term so it is able to analyze datasets in various intensity levels together.

4. Result and Discussion

Analyzed results of horizontal and vertical PGA are shown as an example in Fig. 6 and Fig. 7, respectively. Fig. 6(a) ~ Fig. 6(d) displayed logarithmic amplifications with $Vs30$ in several intensities, i.e. 0.001g, 0.05g, 0.2g, and 0.5g, for horizontal ground motions. The gray dots are all amplifications calculated by Eq. (2) using selected ground motion datasets, whereas the black open squares with error bar show average amplifications in binned $Vs30$. The blue solid line is the regressed model of this study and the green dash



line is the model from Chiou and Youngs [17] performing in four different intensities. Color dots are datasets close to the corresponding intensities. Note that we also plot a black dash line which has only the linear amplification of our model for a reference. Fig. 6(e) ~ Fig. 6(h) displayed logarithmic amplifications with intensity at a reference rock site in several V_{s30} , i.e. 200 m/s, 360 m/s, 760 m/s, and 900 m/s, for horizontal ground motions. The gray dots are all amplifications calculated by Eq. (2) using selected ground motion datasets, whereas the black open squares with error bar show average amplifications in binned reference intensity. Color dots are datasets close to the corresponding V_{s30} . The blue solid line, green dash line, and black dash line are the same as in Fig. 6(a) ~ Fig. 6(d). Fig. 7(a) ~ Fig. 7(h) indicate the same results but for vertical component of ground motions.

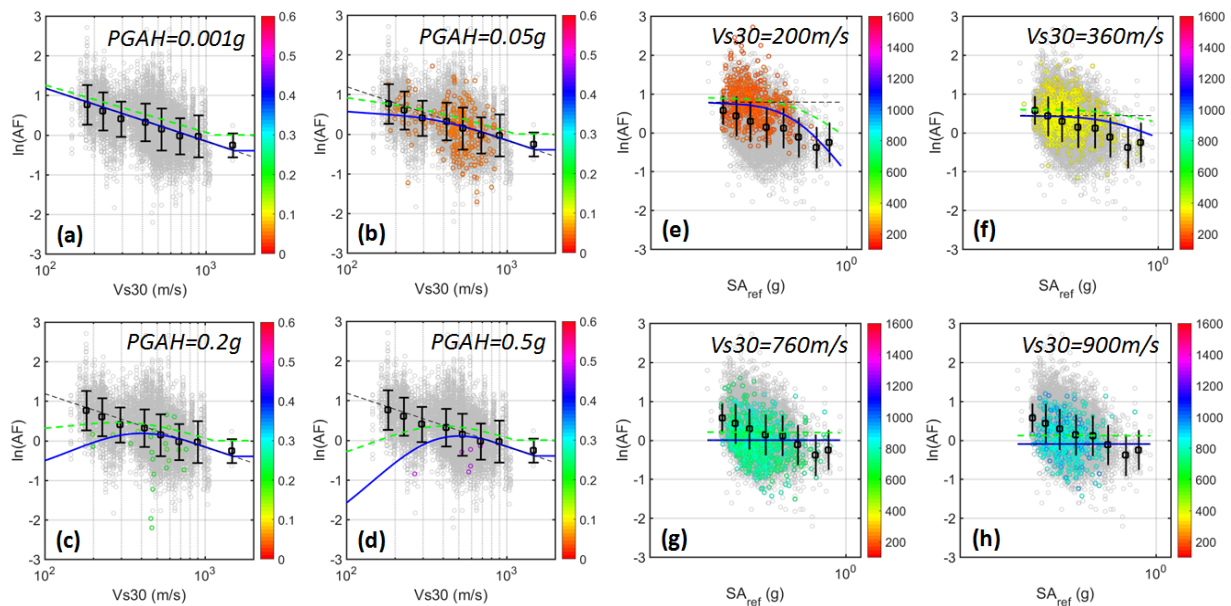


Fig. 6 – Empirical site response model for horizontal PGA using Taiwan data.

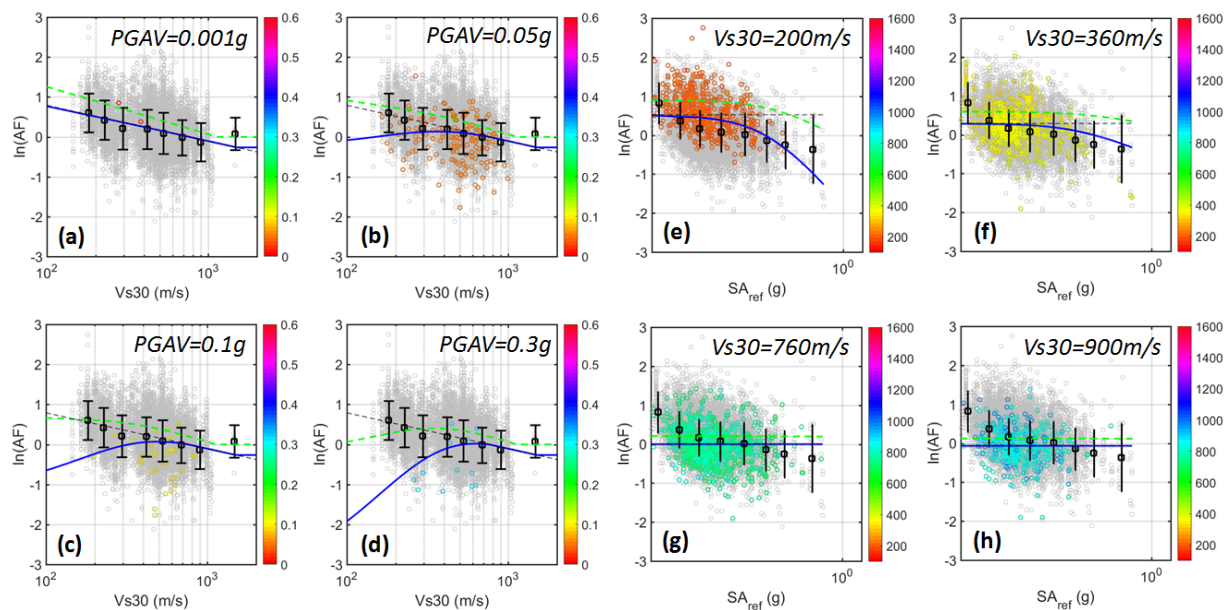


Fig. 7 – Empirical site response model for vertical PGA using Taiwan data.



In Fig. 6(a) ~ Fig. 6(d), the average amplifications (black open squares) looks linear and datasets with smaller V_{s30} has larger amplifications. Our site response model (blue solid line) behaved linear, and started to concave down in lower V_{s30} with increasing intensity. The site response model has no amplification, i.e. amplification factor is 1, in the site condition of V_{s30} equal to 760 m/s according to our design in Eq. (5). Our model also allowed amplification factor smaller than 1 for higher V_{s30} . This means the reference rock site with a condition of V_{s30} equal to 760 m/s. However, the model of Chiou and Youngs [17] use $V_{s30} = 1130$ m/s as a reference rock condition and smaller amplification is not allowed for higher V_{s30} in their model. This is why the flat portion in higher V_{s30} is different in the two models. It should be noted that our model show more obvious deamplifications in larger intensities comparing with the model of Chiou and Youngs. In Fig. 6(e) ~ Fig. 6(h), the average amplifications (black open squares) decrease with increasing reference intensities, that is, the so called nonlinear seismic site response. Evidently, the amplifications decrease with increasing V_{s30} ; otherwise, the decreasing tendency like the black square is clear for those color datasets with smaller V_{s30} but become obscure for those with higher V_{s30} . The vertical site response model shows similar behaviors in Fig. 7(a) ~ Fig. 7 (h) with the horizontal model but smaller linear amplifications.

In order to further confirm the linear and nonlinear site response, we used an alternative approach to capture the behaviors. For each event we used the ground motions at reference rock sites to evaluate an event-specific GMPE, and then the residuals of all stations with records were derived. The residuals are assumed as completely caused by site responses for each site during a single event and therefore can be used to assess linear and nonlinear site responses. An example from one ChiChi aftershock was expressed in Fig. 8. Similar relationships between residuals, V_{s30} , and reference intensity were found as in the Fig. 6. The black squares are the datasets of the reference rock sites and color dots are datasets of corresponding intensities or site conditions. Linear and nonlinear site response identities as described above were found in this figure.

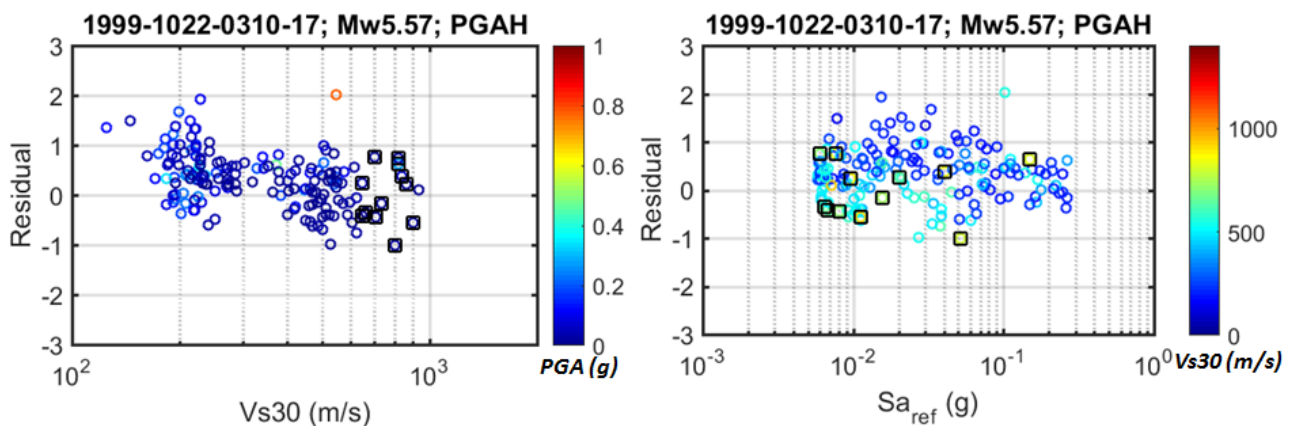


Fig. 8 – Residual distributions for a single event.

5. Conclusions

We proposed a site response model incorporated with both linear and nonlinear terms, which are borrowed from recently GMPEs [16, 17] with modification. NCREC has constructed a strong motion database and the data are used in this study to analyze a site response model for Taiwan. Although most GMPE only developed for horizontal ground motions, we developed site response model for both horizontal and vertical component in this study. Our horizontal site response model show stronger linear and nonlinear behavior than the site response model of a global GMPE [17]. As for the vertical site response model, no other empirical model could be found for comparison because vertical site response is still a challenge. In NGA-



West2 project, both empirical data and analytical simulation were used to constrain the behavior of the nonlinear site response during different site condition and intensities. However, Similar approach is still not available in Taiwan. In addition, this study indicate regional difference of site response behavior between California and Taiwan, but the reason is still unknown. This implies that regional data (both strong motion time history and nonlinear material curves) should be considered in site response studies, rather than just selected data from other regions. A site response analysis without considering local data may be distorted due to regional difference of ground motion and site response.

6. Copyrights

17WCEE-IAEE 2020 reserves the copyright for the published proceedings. Authors will have the right to use content of the published paper in part or in full for their own work. Authors who use previously published data and illustrations must acknowledge the source in the figure captions.

7. References

- [1] Bard, PY Chávez-García FJ (1993): On the decoupling of surficial sediments from surrounding geology at Mexico City. *Bulletin of Seismological Society of America*, **83**, 1979-1991.
- [2] Borcherdt RD (1970): Effect of local geology on ground motion near San Francisco Bay. *Bulletin of the Seismological Society of America*, **60** (1), 29-61.
- [3] Nakamura Y (1989): A method for dynamic characteristics estimation of subsurface using microtremor on the ground surface. *Quarterly Report of RTRI*, **30** (1), 25-33.
- [4] Nakamura Y (2019): What is the Nakamura method? *Seismological Research Letters*, **90** (4), 1437-1443.
- [5] Borcherdt RD (1994): Estimates of site-dependent response spectra for design (methodology and justification). *Earthquake Spectra*, **10** (4), 617-653.
- [6] Building Seismic Safety Council (1998): NEHRP recommended provisions for seismic regulations for new buildings and other structures, 1997 Edition, Part 1: Provisions. *Building Seismic Safety Council for the Federal Emergency Management Agency (Report FEMA 302)*, Washington, D.C.
- [7] Borcherdt RD (2002): Empirical evidence for acceleration-dependent Amplification factors. *Bulletin of the Seismological Society of America*, **92** (2), 761-782.
- [8] National Center for Research on Earthquake Engineering (2015): Reevaluation of Probabilistic Seismic Hazard of Nuclear Facilities in Taiwan Using SSHAC Level 3 Methodology Project. available at <http://sshac.ncree.org.tw>.
- [9] Liu KS, Shin TC, Tsai YB (1999): A free-field strong motion network in Taiwan: TSMIP. *Terrestrial, Atmospheric and Oceanic Sciences*, **10** (2), 377-396.
- [10] Boore DM (2010): Orientation-Independent, Nongeometric-Mean Measures of Seismic Intensity from Two Horizontal Components of Motion. *Bulletin of the Seismological Society of America*, **100**(4), 1830–1835.
- [11] Kuo CH, Wen KL, Hsieh HH, Lin CM, Chang TM, Kuo KW (2012): Site classification and V_{s30} estimation of free-field TSMIP stations using the logging data of EGDT. *Engineering Geology*, **129-130**, 68-75.
- [12] Kuo CH, Lin CM, Chang SC, Wen KL, Hsieh HH (2017): Site Database for Taiwan Strong Motion Stations. *Technical Report NCREE*, No. NCREE-17-004.
- [13] Kuo CH, Chen CT, Lin CM, Wen KL, Huang JY, Chang SC (2016): S-wave velocity structure and site effect parameters derived from microtremor arrays in the western plain of Taiwan. *Journal of Asian Earth Sciences*, **128**, 27-41.
- [14] Kwok OLA, Stewart JP, Kwak DY, Sun PL (2018): Taiwan-specific model for V_{s30} prediction considering between-proxy correlations. *Earthquake Spectra*, **34** (4), 1973-1993.
- [15] Lin CM, Kuo CH, Huang JY, Hsieh HH, Si CC, Wen KL (2018): Shallow Shear-Wave Velocity Structures of TSMIP Stations in Taiwan. *Technical Report NCREE*, No. NCREE-18-019.



- [16] Abrahamson NA, Silva WJ, Kamai R (2014): Summary of the ASK14 ground motion relation for active crustal regions. *Earthquake Spectra*, **30**(3), 1025-1055.
- [17] Chiou BSJ Youngs RR (2014): Update of the Chiou and Youngs NGA model for the average horizontal component of peak ground motion and response spectra. *Earthquake Spectra*, **30**(3), 1117-1153.
- [18] Seyhan E, Stewart JP (2014): Semi-Empirical Nonlinear Site Amplification from NGA-West2 Data and Simulations. *Earthquake Spectra*, **30**(3), 1241-1256.